RSC Advances

PAPER

View Article Online
View Journal | View Issue

Cite this: *RSC Adv.*, 2025, **15**, 7563

Au supported on γ-AlOOH and γ-Al_2O_3 for low temperature oxidation of CO and aromatic alcohols†

Zongbo Shi, *[a] Qing Zhang,[a] Guangpeng Yang,[a] Liang Liu,[a] Gang Wang,[b] Rizki Ekananda,[c] Ismal Gamar,[c] Ruilin Wang[b] and Runsheng Zhuo*[a]

Received 22nd January 2025
Accepted 3rd March 2025

DOI: 10.1039/d5ra00527b

rsc.li/rsc-advances

0.5%Au supported on γ-AlOOH and γ-Al_2O_3 was used for low temperature oxidation of CO and aromatic alcohols. Various characterization techniques, including X-ray diffraction, N_2 adsorption, FT-IR spectroscopy, XPS, TEM, CO_2-TPD and solid-state MAS NMR, were employed to characterize these catalysts. The Au/γ-AlOOH sample has abundant hydroxyl groups and basic sites on its surface, exhibiting strong adsorption for aromatic alcohols, and outstanding activity for low-temperature oxidation of aromatic alcohols. The Au/γ-Al_2O_3 sample shows sufficient Au^+ sites leading to high performance for low-temperature CO oxidation.

1 Introduction

Small Au nanoparticles have attracted considerable attention in the last few decades due to their high activity for catalytic oxidation of various reactions.[1,2] Low temperature oxidation of carbon monoxide is the classical example of gold catalysis, as first reported by Haruta and co-workers in 1987.[3,4] Recently, low temperature oxidation of alcohol on Au nanoparticles using molecular oxygen as an oxidant to the corresponding aldehydes, ketones and acids has met the demand of green synthesis of organic products.[5–9]

The support can influence catalyst activity by participating in the reaction. For example, the synergetic catalysts of Au nanoparticles and alkaline metal oxide support promote the oxidation activity of both alcohol and CO. Costa *et al.* found that using MgO as a support for preparing gold catalysts enables the effective oxidation of a wide range of alcohols with molecular oxygen as the sole oxidant.[10] Schüth and his coworkers synthesized gold supported on MgO, which exhibited unprecedented oxidation activity for CO even at −89 °C.[11] The support can also influence the catalytic activity as it affects parameters, such as the Au particle size, Au oxidation state, and metal–support interaction.[12] Reducible oxides such as TiO_2, ZrO_2, Fe_2O_3, CeO_2 and Co_3O_4 are considered most active because of their excellent ability to provide reactive oxygen to the active gold sites.[1,13] TiO_2 has been reported to reduce the size of Au nanoparticles, which results in high oxidation activity of CO.[14–16] The metal–support interaction between Au and the CeO_2 support has also been reported, which indicated high oxidation activity of alcohol and CO.[17–21] The ionic states of supported gold were stabilized by the cerium oxide and Au^+ cations were claimed as the active sites in the partial oxidation of alcohols.[17,18] Corma and coworkers prepared a nanocrystalline CeO_2 support, which enhances the activity of Au for CO oxidation by two orders of magnitude compared to the catalysts prepared using conventional CeO_2 support, by influencing the surface electronic properties and, consequently, the gold–support interaction.[21]

Hydroxy groups and alkalinity of support are also known to influence the stability and activity of catalytic Au nanoparticles.[22–24] γ-Al_2O_3 is the most commonly used noble metal catalyst carrier due to its large specific surface area, which is usually obtained by interlayer dehydroxylation of γ-AlOOH at temperatures of 450–750 °C.[25] γ-Al_2O_3 and γ-AlOOH carriers have significant differences in hydroxyl groups, surface Al^{3+}, acidity as well as alkalinity. Huang *et al.* claimed that the strong alkaline sites on the surface of γ-AlOOH enable Au/γ-AlOOH to exhibit high activity in the oxidation of α,ω-diols, despite its gold particle size being much larger than that of Au/γ-Al_2O_3.[24] The morphology of Al_2O_3 support also affects the activity of catalytic Au nanoparticles. Recently, the thin porous Al_2O_3 sheets were reported as exceptional catalyst supports for Au nanoparticles, exhibiting high activity for low-temperature CO oxidation and stabilizing Au nanoparticles at annealing temperatures up to 900 °C.[26] The Au particle size and water vapor in the atmosphere is crucial for the low temperature CO oxidation performance of Au/Al_2O_3 catalysts,[27–29] Moroz *et al.* discovered that the Au/Al_2O_3 catalysts containing Au particles

[a]*REZEL Catalysts Corp., Shanghai, 201313, China. E-mail: zongbo.shi@rezel.com.cn; Fax: +86-21-38280081*

[b]*College of Materials Science and Engineering, Sichuan University, Chengdu 610065, China*

[c]*PT Pertamina (Persero), East Jakarta, 13920, Indonesia*

† Electronic supplementary information (ESI) available. See DOI: https://doi.org/10.1039/d5ra00527b

with a diameter of ≤5 nm demonstrate remarkable catalytic activity for the oxidation of CO when water vapor is present under near-ambient conditions.[29]

Here we present an unexpected result for CO and aromatic alcohols oxidation with Au/γ-AlOOH and Au/γ-Al_2O_3 as catalysts. The Au/γ-AlOOH exhibits higher aromatic alcohols oxidation activity than that of Au/γ-Al_2O_3 catalyst, while Au/γ-Al_2O_3 exhibits higher CO oxidation activity. We also investigated the effects of support and Au oxidation state on the oxidation of CO and aromatic alcohols.

2 Experimental

2.1 Chemicals

$NaAlO_2$ (Al_2O_3, 54.09 wt%; Na_2O, 40.44 wt%) were purchased from J&K Chemical Ltd. Sodium bicarbonate, ammonium sulphate, ethanol (EtOH), $HAuCl_4$ and KBH_4 all in AR grade, were supplied by Sinopharm Chemical Reagent Co. Ltd. The chemicals were used as received, without further purification.

2.2 Preparation of boehmite (γ-AlOOH) and γ-alumina (γ-Al_2O_3)

The hierarchically structured boehmite and γ-alumina supports with a flower-like morphology were synthesized taking bayerite as the starting raw materials following the reference.[30]

Typical synthesis of bayerite was as follows: 20.1 g $NaAlO_2$ was dissolved in 134.0 g of hot water, stirred and then cooled to room temperature. After that, 190 mL of 1 mol L^{-1} $NaHCO_3$ solution was added drop-wise to the above solution. A white suspension was formed. The suspension was agitated for about 6 h, then filtered and washed thoroughly with hot water. The resulting filter cake was then dried at 80 °C overnight.

Typical syntheses of hierarchically structured boehmite and alumina were as follows: A mixture of 0.8 g bayerite, 0.6 g $(NH_4)_2SO_4$, 2.7 g H_2O and 2.3 g EtOH was placed in a 25 mL Teflon-lined stainless-steel autoclave, heated to 175 °C, maintained at the temperature for 12 h, and then cooled down naturally. The obtained white solid was recovered by filtration, washed with hot water, and dried at 80 °C overnight. The product was denoted as γ-AlOOH. The γ-Al_2O_3 sample was obtained by calcination of the γ-AlOOH at 550 °C for 6 h with a heating rate of 2 °C min^{-1}.

2.3 Supporting 0.5%Au on the γ-AlOOH and γ-Al_2O_3

The Au/γ-AlOOH or Au/γ-Al_2O_3 was prepared as follows:

10 g γ-AlOOH or γ-Al_2O_3 was added into a vessel (50 mL) containing 25 mL of 0.01 mol L^{-1} $HAuCl_4$ and stirred for 2 min. Subsequently, a 5% $NH_3 \cdot H_2O$ solution was added dropwise to adjust the pH of the suspension to 8–9. The suspension was further stirred for 2 h. Then, 0.27 g of KBH_4 was added to reduce the Au^{3+} species. The obtained solid was filtered, washed with deionized water, and dried under vacuum overnight.

2.4 CO oxidation testing

The CO oxidation reaction was performed in a continuous flow fixed-bed quartz reactor under atmospheric pressure. A 0.2 g (40–60 mesh) sample was loaded and pre-treated with a 20 vol% O_2/He mixture (50 mL min^{-1}) at 100 °C for 30 min. After cooling down to 20 °C, a gas mixture with 1.0 vol% CO/2.5 vol% O_2/He (50 mL min^{-1}) was introduced. Moisture was controlled by passing the feed gas through a soda lime tube. The concentrations of CO, CO_2 and O_2 in the outlet streams were measured using an on-line gas chromatograph.

2.5 1-Phenylethanol, benzyl alcohol and 4-methoxybenzyl alcohol oxidation testing

The oxidations of aromatic alcohols (1-phenylethanol, benzyl alcohol, or 4-methoxybenzyl alcohol) were carried out in a 25 mL glass reactor equipped with a reflux condenser and a magnetic stirrer. In a typical reaction, 100 mg of catalyst, 1 mmol of aromatic alcohols and 5 mL of tetradecane were introduced into the reactor. The air flow rate was 60 mL min^{-1}, the string rate was 350 rpm, and the mixture was heated to 40∼70 °C and maintained at this temperature for 6∼8 h. 0.5 mmol 1,3,5-triisopropylbenzene was used as an internal standard. The liquid samples were analyzed using a Shimadzu GC-2014 gas chromatograph equipped with a 30 m DB-Wax capillary column and an FID detector.

2.6 Characterization methods

Powder X-ray diffraction (XRD) patterns were collected on a Rigaku-Ultima diffractometer using a Cu Kα radiation source ($\lambda = 0.15432$ nm) in the 2θ range from 5° to 80°. Transmission electron microscopic images were conducted on TECNAI G2 F30 operating at 300 kV after the specimens were dispersed in ethanol and deposited on holey copper grids. N_2 adsorption–desorption isotherms were measured at −196 °C on a Quanta chrome Autosorb-3B volumetric adsorption analyzer. Before the measurements, the samples were outgassed in the degas port of the adsorption apparatus at 150 °C for 6 h. BET specific surface area was calculated using adsorption data acquired at a relative pressure (P/P_0) range of 0.05–0.30 and the total pore volume determined from the amount adsorbed at P/P_0 of about 0.99. Pore size distribution (PSD) curves were calculated from the adsorption isotherm branches using the Barrett–Joyner–Halenda (BJH) algorithm. Au contents were determined by inductively coupled plasma optical emission spectrometry (ICP-OES) on a Thermo IRIS Intrepid II XSP atomic emission spectrometer. Surface electronic state of Au was also evaluated using X-ray photoelectron spectroscopy (XPS) measurements with a Thermo Fisher Scientific ESCALAB 250Xi spectrometer with Al Kα radiation (1486.6 eV) as incident beam with a monochromator. All the spectra were obtained at room temperature, and the binding energies of elements were referenced to the adventitious C1s peak at 284.8 eV. ^{27}Al MAS NMR spectra were measured on a VARIAN VNMRS 400WB NMR spectrometer.

Temperature-programmed desorption of CO_2 (CO_2-TPD) testing was performed using a TP-5080 chemisorption instrument (Xianquan Co., Ltd, Tianjin, China) with a thermal conductivity detector (TCD). After pretreatment of each sample (100 mg) at 200 °C under flowing helium (25 mL min^{-1}) for 2 h, the sample was cooled to 50 °C, and then adsorbed to saturation

by introducing 10 vol% CO_2/He (25 mL min^{-1}) mixture for 10 min. CO_2 physically adsorbed on the catalyst was removed by flushing the sample with helium (25 mL min^{-1}) for 20 min. Thermal desorption of CO_2 was carried out in the temperature range of 50∼200 °C increasing at a rate of 10 °C min^{-1}.

Infrared (IR) spectra were recorded on a Nicolet Fourier transform infrared spectrometer (NEXUS 670). The self-supported wafers (about 10 mg, Φ 1 cm) were pretreated in the IR cell under vacuum at the temperature from 20 °C to 550 °C for 10 min and then the IR spectra of OH group were recorded. For IR spectra of absorbed 1-phenylethanol, the self-supported wafers were pretreated in the IR cell under vacuum at 200 °C for 10 min, after the samples were cooled down to room temperature, 1-phenylethanol vapor dozed into the IR cell. IR spectra of absorbed 1-phenylethanol were recorded under vacuum at the temperature from 20 °C to 200 °C for 10 min.

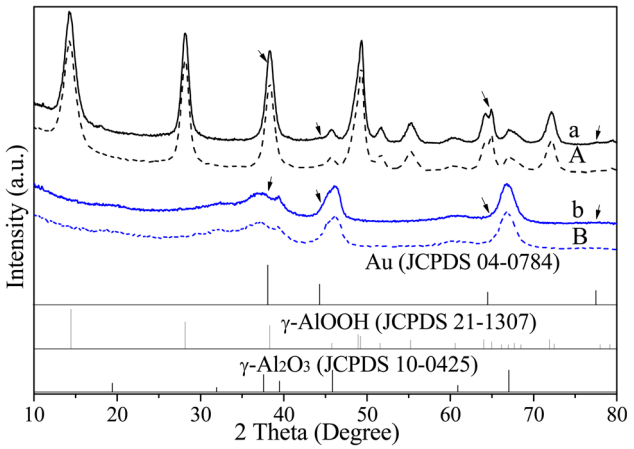

Fig. 1 Wide-angle XRD patterns of the as-synthesized γ-AlOOH (A, dotted line), Au/γ-AlOOH (a, solid line), γ-Al_2O_3 (B, dotted line) and Au/γ-Al_2O_3 (b, solid line). The arrows mark reflexes from Au particles.

3 Results and discussions

3.1 Characterization of Au/γ-AlOOH and Au/γ-Al_2O_3 samples

The wide-angle XRD patterns of the Au/γ-AlOOH and Au/γ-Al_2O_3 are shown in Fig. 1. The diffraction peaks at 14.48°, 28.18°, 38.34° and 48.93° are related to boehmite phase (JCPDS no. 21-1307).[31] The γ-Al_2O_3 structure (JCPDS no. 10-0425) is formed by calcining γ-AlOOH at 550 °C.[32] No peaks related to the Au phase were observed, suggesting low Au concentration and small particle size, with the Au diffraction peaks overlapping with the strong peaks of γ-AlOOH and γ-Al_2O_3.

Fig. 2 shows the TEM images of Au/γ-AlOOH (left) and Au/γ-Al_2O_3 (right) samples. The shape of primary nanosheet (1–5 nm thick) particles of γ-AlOOH is preserved after conversion to γ-Al_2O_3 by calcination. Au nanoparticle can be observed in both samples, the average particle sizes of Au/γ-AlOOH sample and Au/γ-Al_2O_3 sample are 4.6 nm and 4.4 nm, respectively.

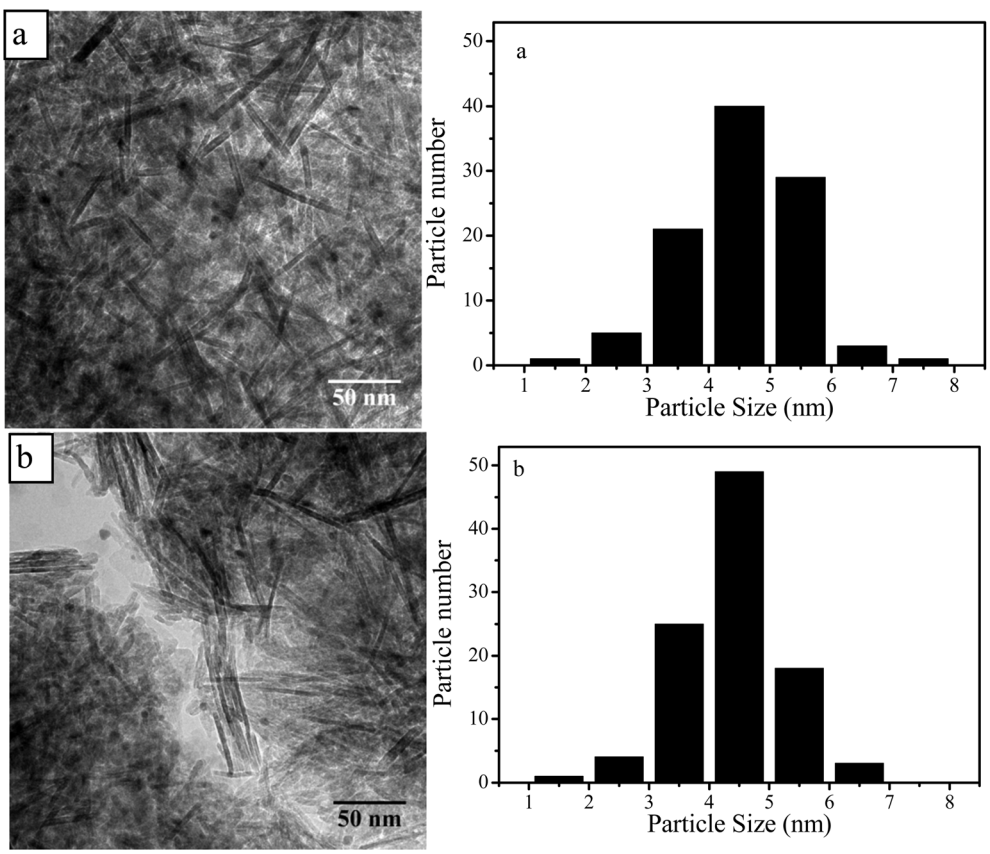

Fig. 2 TEM images (left) and Au particle size distribution (right) of the as-synthesized Au/γ-AlOOH (a) and Au/γ-Al_2O_3 (b).

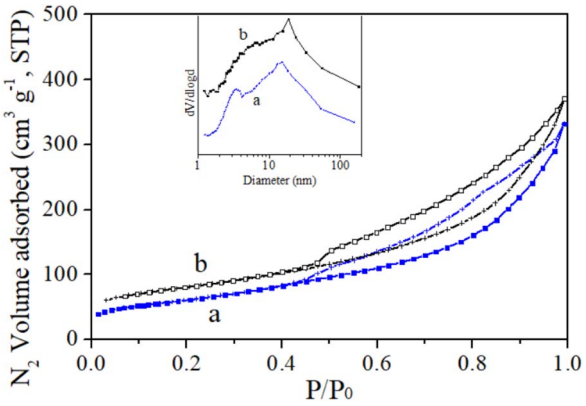

Fig. 3 N_2 adsorption/desorption isotherms and pore size distribution curves (insert) of the as-synthesized Au/γ-AlOOH (a) and Au/γ-Al_2O_3 (b) samples. The curves (b) are offset a little for clarity.

Fig. 3 presents the N_2 adsorption/desorption isotherms and pore size distribution curves of the Au/γ-AlOOH and Au/γ-Al_2O_3 samples. Both Au/γ-AlOOH and Au/γ-Al_2O_3 samples show typical characteristics of type IV isotherms with the hysteresis loop, where the adsorbed amount increases continuously with rising P/P_0.[33]

Table 1 summarizes the surface areas, total pore volumes and the pore diameters of the Au/γ-AlOOH and Au/γ-Al_2O_3 samples. The surface area of the Au/γ-AlOOH sample is 217 m^2 g^{-1} and the total pore volume is 0.48 cm^3 g^{-1}. The surface area of the Au/γ-Al_2O_3 is 279 m^2 g^{-1}, and the total pore volume is 0.58 cm^3 g^{-1}. Both the surface area and pore volume of Au/γ-Al_2O_3 are higher than those of the Au/γ-AlOOH. Both the samples exhibit bimodal pore size distribution.[34] The Au/γ-AlOOH sample has the peaks centered at 3.4 nm and 15.9 nm, respectively and the Au/γ-Al_2O_3 sample has those at 6.3 nm and 18.9 nm, respectively.

Fig. 4 gives ^{27}Al NMR spectra of as-synthesized γ-AlOOH, Au/γ-AlOOH, γ-Al_2O_3 and Au/γ-Al_2O_3 samples. The resonance at ~10 ppm is associated with octahedrally coordinated aluminum. Additional peaks at ~68 ppm and ~38 ppm are observed in the spectra of γ-Al_2O_3 and Au/γ-Al_2O_3 samples, indicating generation of tetrahedrally and pentahedrally coordinated aluminum after calcination of boehmite.[35] Similar spectra were observed between the support and Au-loaded samples, suggesting that the addition of Au does not alter the support's structure.

The valences of Au species in Au/γ-AlOOH and Au/γ-Al_2O_3 samples are investigated by using XPS. As shown in Fig. 5, Au 4f

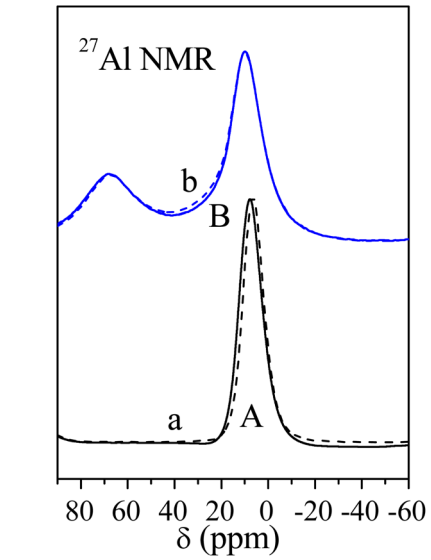

Fig. 4 ^{27}Al NMR spectra of as-synthesized γ-AlOOH (A, dotted line), Au/γ-AlOOH (a, solid line), γ-Al_2O_3 (B, dotted line) and Au/γ-Al_2O_3 (b, solid line).

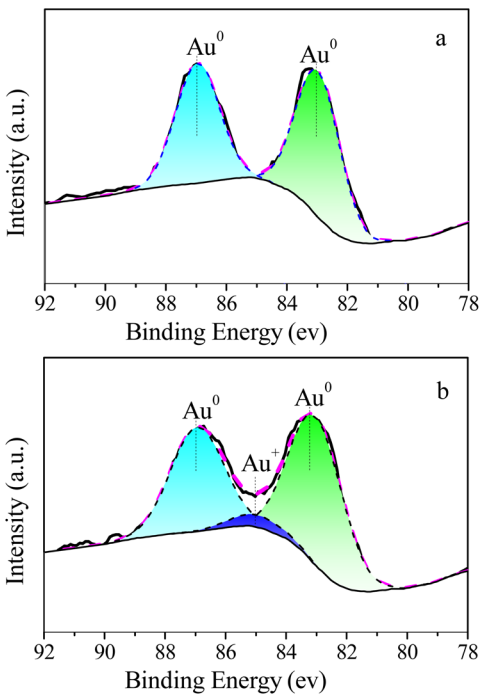

Fig. 5 Au 4f XPS spectra of Au/γ-AlOOH (a) and Au/γ-Al_2O_3 (b).

Table 1 Textual properties of the Au/γ-AlOOH and Au/γ-Al_2O_3 samples

No.	Sample	S_{BET} (m^2 g^{-1})	V_{total} (cm^3 g^{-1})	d_{BJH}[a] (nm)
1	Au/γ-AlOOH	217	0.48	3.4/15.9
2	Au/γ-Al_2O_3	279	0.58	6.3/18.9

[a] The pore size is derived from the adsorption isotherm by BJH method.

peaks are chosen to compare the valence of Au in Au/γ-AlOOH and Al–Al_2O_3 samples. Both the Au/γ-AlOOH and Au/γ-Al_2O_3 samples exhibit the presence of Au^0 species on the catalyst surface.[36] The Au/γ-Al_2O_3 sample shows particular Au^+ species, compared with the Au/γ-AlOOH sample. Casaletto *et al.* claimed that presence of Au^+ species is the main requisite for achievement of the highest CO conversion at the low temperatures.[17]

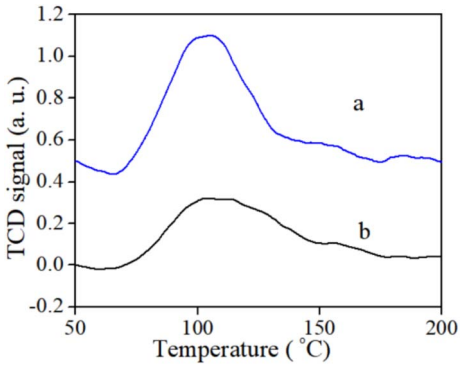

Fig. 6 CO_2-TPD profiles of Au/γ-AlOOH (a) and Au/γ-Al_2O_3 (b).

The alkalinity properties and total amounts of basic sites are investigated by using CO_2 temperature-programmed desorption (CO_2-TPD) technique. As shown in Fig. 6, Au/γ-AlOOH and Au/γ-Al_2O_3 samples display similar CO_2 desorption at 110 °C, which is due to the desorption of CO_2 on the weak basic sites.[24] According to the peak areas of CO_2 desorption in the two samples, the total basic sites of Au/γ-AlOOH are 1.6 times higher than that of Au/γ-Al_2O_3. Ide *et al.* proposed that adsorbed hydroxyl groups can activate O–H and C–H bonds, thereby increasing the oxidation rate of glycerol, even bulk gold powder becomes an active oxidation catalyst in alkaline water.[37] Tang *et al.* found that alkali metal dopants were found to significantly delay total oxidation of CO over Co_3O_4 nano-catalyst,[38] Gluhoi *et al.* found that alkali (earth) metal oxide additives act as structural promoters, which may contribute to the activation of O_2 during the low-temperature oxidation of CO.[39]

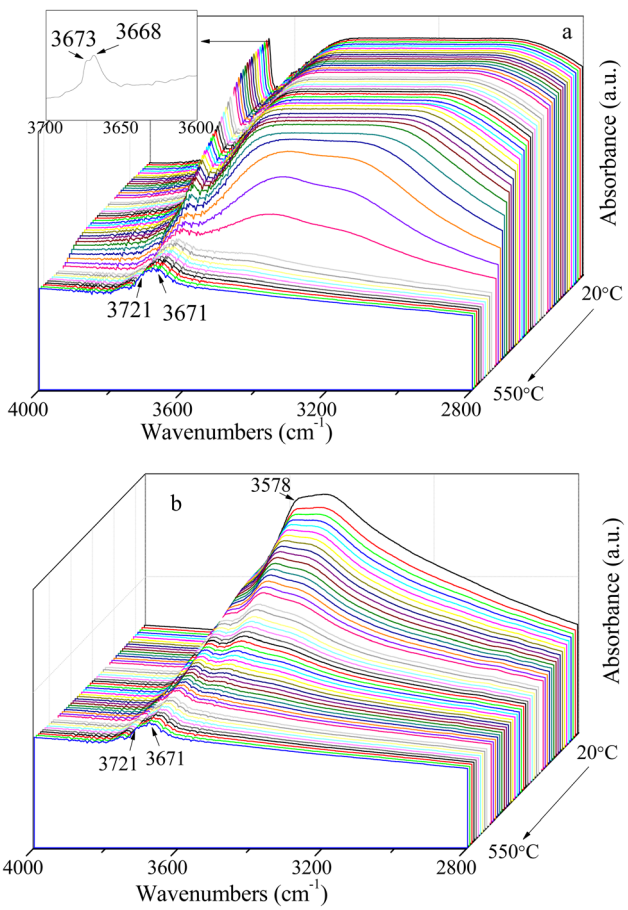

Fig. 7 Change of IR spectra (OH region) of the Au/γ-AlOOH (a) and Au/γ-Al_2O_3 (b) as a function of temperature.

Fig. 7 displays the OH stretching vibrations between 2800 cm^{-1} and 4000 cm^{-1} for the Au/γ-AlOOH and Au/γ-Al_2O_3 samples. Two characteristic absorption bands of OH groups of Au/γ-AlOOH were observed at 3673 cm^{-1} and 3668 cm^{-1}. A broad flat peak attributed to the skeletal Al–OH of γ-AlOOH were observed at 2960∼3480 cm^{-1}. The Au/γ-Al_2O_3 showed three bands at 3721 cm^{-1}, 3671 cm^{-1}, 3578 cm^{-1}, which attributes to the absorption bands of OH groups of γ-Al_2O_3. Under vacuum condition of 20 °C and 50 °C, the absorption bands of OH groups in Au/γ-AlOOH are much higher than that in Au/γ-Al_2O_3. As the temperature increases, γ-AlOOH gradually transforms into γ-Al_2O_3, and the surface Al–OH in γ-AlOOH gradually disappears. After vacuum treatment of 550 °C, the IR spectrum (OH region) of the Au/γ-AlOOH and Au/γ-Al_2O_3 is basically the same, which is due to the conversion of γ-AlOOH to γ-Al_2O_3.[40]

The surface properties of the Au/γ-AlOOH and Au/γ-Al_2O_3 samples are further examined by the 1-phenylethanol adsorption. Fig. 8 displays IR spectra of 1-phenylethanol adsorbed on the Au/γ-AlOOH and Au/γ-Al_2O_3 samples. Both Au/γ-Al_2O_3 and Au/γ-AlOOH samples exhibit the peaks at 1400–1650 cm^{-1}, which is attributed to the aromatic C=C stretching vibrations from the benzene ring and α-deformation (bending vibrations) of the CH_3 group.[41–43] In addition, the Au/γ-AlOOH sample shows more 1-phenylethanol absorption peak than the Au/γ-Al_2O_3 sample, as shown in Table 2, which is consistent with the IR spectra (OH region) results. At 50 °C, the area of 1-phenylethanol absorption peak at 1443 cm^{-1} of Au/γ-AlOOH is 3.32 times that of Au/γ-Al_2O_3. Higher alcohol adsorption capacity helps to enhance alcohol oxidation activity.

3.2 Catalytic properties of Au/γ-AlOOH and Au/γ-Al_2O_3 samples in CO oxidation

The Au/γ-AlOOH and Au/γ-Al_2O_3 samples are tested for CO oxidation at 20 °C under a reaction stream with a gas composition of 1.0 vol% CO/2.5 vol% O_2/He mixture. The conversion *vs.* reaction time is shown in Fig. 9. The initial CO conversions of the Au/γ-Al_2O_3 and Au/γ-AlOOH samples are 82% and 26%, respectively. The CO oxidation performance of the Au/γ-Al_2O_3 sample is much superior than that of the Au/γ-AlOOH sample. XPS spectra suggest that the Au/γ-Al_2O_3 sample contains more Au^+ species than the Au/γ-AlOOH sample, which is favorable for CO_2 forming. XPS spectra suggest that the Au/γ-Al_2O_3 sample has more Au^+ species than those the Au/γ-AlOOH sample has, which is favorable for CO_2 forming. These results lead to the outstanding CO oxidation performance of Au/γ-Al_2O_3, as shown in Scheme 1. Then, the catalytic performance of these samples tends to reduce, CO conversions of the Au/γ-Al_2O_3 and Au/γ-AlOOH samples decreased to about 50% and 8% after 450 hours, respectively. This result is in good agreement with the

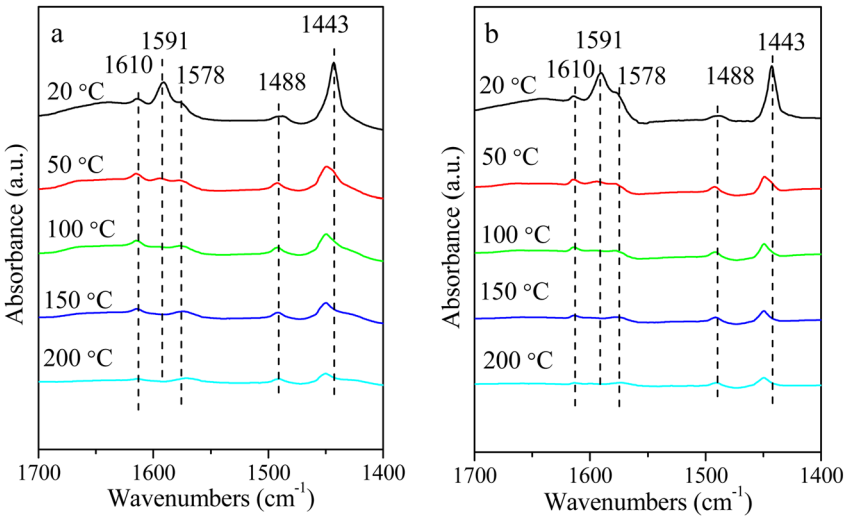

Fig. 8 IR spectra of 1-phenylethanol absorbed on Au/γ-AlOOH (a) and Au/γ-Al_2O_3 (b), all samples were normalized by subtracting the peak of the vacuum adsorption sample at 200 °C.

Table 2 The area of 1-phenylethanol absorption peak at 1443 cm^{-1} for the samples Au/γ-AlOOH (a) and Au/γ-Al_2O_3 (b)

Desorption temp. (°C)	Peak area (1443 cm^{-1})	
	Au/γ-AlOOH	Au/γ-Al_2O_3
20	8.7	5.0
50	6.3	1.9
100	5.2	1.7
150	4.3	1.4
200	2.8	1.0

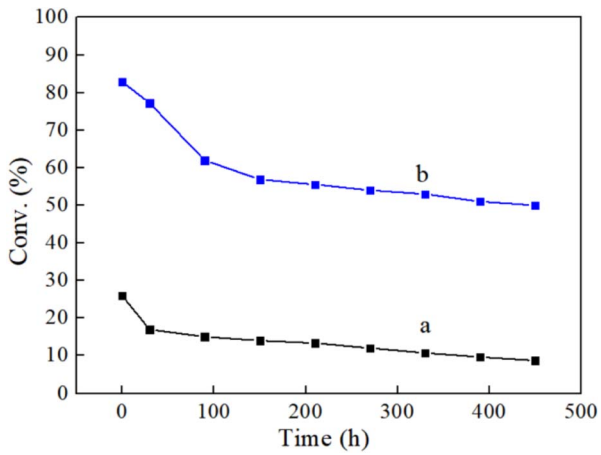

Fig. 9 The CO conversion of Au/γ-AlOOH (a) and Au/γ-Al_2O_3 (b) samples.

literature data,[29] they hypothesized that the CO + O_2 reaction occurs by inserting adsorbed CO molecules into the Au^{x+}–OH complex to form carboxylate species, and the presence of water vapor is crucial for maintaining sufficient concentrations of Au^{x+}–OH species.[29,44] Therefore, the absence of water vapor will lead to a decrease in CO activity over time.

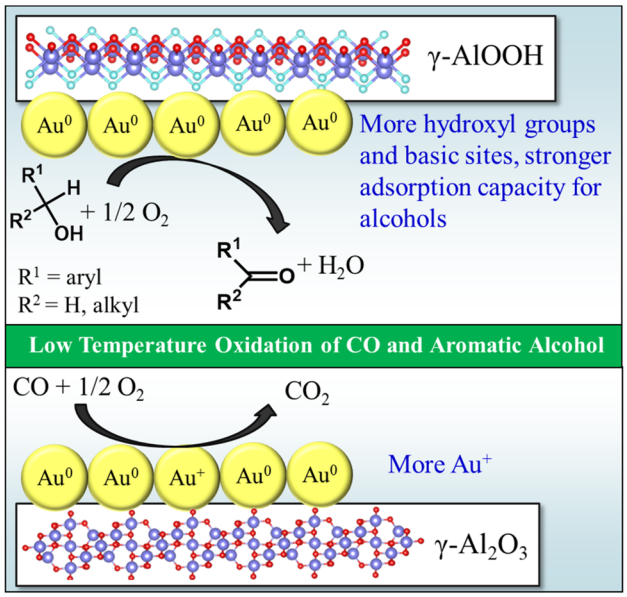

Scheme 1 Proposed reaction mechanism for the oxidation of CO and alcohol over Au/γ-AlOOH and Au/γ-Al_2O_3 samples.

3.3 Catalytic properties of Au/γ-AlOOH and Au/γ-Al_2O_3 samples in oxidation of alcohols

The selective oxidation of alcohols is one of the most important and fundamental transformations in organic synthesis, acted as the versatile intermediates of valuable compounds such as pharmaceuticals, agricultural chemicals, and fine chemicals. We use 1-phenylethanol, benzyl alcohol and 4-methoxybenzyl alcohol oxidation as the probe reaction of aromatic alcohols oxidation. Table 3 gives the conversion of 1-phenylethanol, benzyl alcohol and 4-methoxybenzyl alcohol oxidation on the Au/γ-AlOOH and Au/γ-Al_2O_3 samples, all reactions display about 100% selectivity, no other by-products can be detected.

Table 3 The conversion of 1-phenylethanol, benzyl alcohol and 4-methoxybenzyl alcohol oxidation of Au/γ-AlOOH and Au/γ-Al_2O_3 samples

Entry	Substrate	Product	Temp. (°C)	Time (h)	Conv. (%) Au/γ-AlOOH	Conv. (%) Au/γ-Al_2O_3
1			40	6	73.0	32.1
2			70	8	32.6	16.9
3	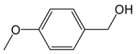	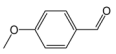	70	6	25.4	14.8

Au/γ-AlOOH sample display a conversion of 73.0% for 1-phenylethanol oxidation at 40 °C for 6 h. Chen *et al.* claimed a conversion of 82% and selectivity of 90% for 1-phenylethanol oxidation over Pd/SiO_2–Al_2O_3–H_2 catalyst at 150 °C for 24 h,[45] and Yamaguchi *et al.* reported a conversion of >99% and selectivity of >90% over Ru/Al_2O_3 at 83 °C for 1 h.[46] Herein, 1-phenylethanol can be almost completely oxidized over Au/γ-AlOOH at 40 °C for 6 h, which must be energy saving and eco-friendly. This result shows some advantages of flower-like AlOOH as support catalysis in the alcohols oxidation. Au/γ-AlOOH sample is also suitable for the oxidation of benzyl alcohol and 4-methoxybenzyl alcohol.

The carrier morphology of Au/γ-AlOOH and Au/γ-Al_2O_3 samples is similar, and both samples exhibit a low Au concentration and small Au particle size. The Au/γ-AlOOH sample demonstrates much higher 1-phenylethanol, benzyl alcohol and 4-methoxybenzyl alcohol oxidation conversion than the Au/γ-Al_2O_3 sample does. This result shows some advantages of the Au/γ-AlOOH sample in the alcohols oxidation. IR spectra of OH regions and 1-phenylethanol adsorption indicate the abundant hydroxyl groups and strong adsorption capacity for alcohols of the Au/γ-AlOOH sample. Jiang *et al.* speculated through theoretical calculations that the –OH groups promote chemisorption of alcohol molecules on a gold cluster surface as the initial step of their oxidation by a gold cluster,[47] which is confirmed by our experimental results.

3.4 Influence of support and Au oxidation state on catalytic properties

Scheme 1 exhibits the proposed reaction mechanism for the oxidation of CO and alcohol over Au/γ-AlOOH and Au/γ-Al_2O_3 samples. Au/γ-AlOOH and Au/γ-Al_2O_3 samples exhibit a low Au concentration and small Au particle size, and both samples can be used for low-temperature oxidation of CO and aromatic alcohols. During alcohol oxidation, both the carrier and gold significantly influence the reaction. The hydroxyl groups and basic sites in the carrier sometimes have a greater impact on alcohol oxidation than Au. Ide *et al.* proposed that bulk gold powder acts as an active catalyst for alcohol oxidation in alkaline medium.[37] The Au/γ-AlOOH sample contains a large amount of OH and alkalinity, and has strong adsorption capacity for aromatic alcohols, thus exhibiting excellent low temperature oxidation activity for aromatic alcohols. Au/γ-Al_2O_3 possesses a large amount of Au^+ which is effective in promoting the low temperature CO oxidation.[17]

4 Conclusions

Au/γ-AlOOH and Au/γ-Al_2O_3 samples with low Au concentrations and small Au particle sizes were synthesized for low-temperature oxidation of CO and aromatic alcohols. Under low temperature conditions, the CO oxidation conversion by the Au/γ-Al_2O_3 sample is about three times that of the Au/γ-AlOOH sample, while the oxidation conversions of 1-phenylethanol, benzyl alcohol, and 4-methoxybenzyl alcohol by the Au/γ-Al_2O_3 sample are only about half of those by the Au/γ-AlOOH sample.

The high oxidation activity of Au/γ-AlOOH sample towards 1-phenylethanol, benzyl alcohol, and 4-methoxybenzyl alcohol is mainly due to its rich content of hydroxyl groups and basic sites, which facilitate the adsorption of aromatic alcohols. The high CO oxidation activity of the Au/γ-Al_2O_3 sample is primarily attributed to the efficient Au^+ sites.

Data availability

All relevant data are within the main article.

Conflicts of interest

There are no conflicts to declare.

Acknowledgements

This work was supported by the Panxi Experimental Zone Key Scientific and Technological Project, and National Key Research and Development Program Nanotechnology Specific Project (No. 2020YFA0210900). We are very grateful to Dr Xinsheng Liu and Dr Yimeng Wang for their professional knowledge and insightful comments, which have made significant contributions to the success of this study.

References

1 M. Alhumaimess, Z. Lin, Q. He, L. Lu, N. Dimitratos, N. F. Dummer, M. Conte, S. H. Taylor, J. K. Bartley,

C. J. Kiely and G. J. Hutchings, *Chem.–Eur. J.*, 2014, **20**, 1701–1710.
2 A. Villa, A. Gaiassi, I. Rossetti, C. L. Bianchi, K. van Benthem, G. M. Veith and L. Prati, *J. Catal.*, 2010, **275**, 108–116.
3 M. Haruta, *Nature*, 2005, **437**, 1098–1099.
4 M. Haruta, T. Kobayashi, H. Sano and N. Yamada, *Chem. Lett.*, 1987, **16**, 405–408.
5 P. Rodriguez, Y. Kwon and M. T. M. Koper, *Nat. Chem.*, 2012, **4**, 177–182.
6 A. Ali, D. J. Jasim, N. Rakhimov, M. J. Mohammed, M. M. Karim, A. H. Athab, A. Kumar, N. Ahmad and L. Guo, *J. Mol. Struct.*, 2025, **1319**, 139373.
7 A. Ali, M. K. Abdulameer, M. H. Mahdi, K. H. Rasool, M. S. Jabir, F. H. Zankanah, H. Majdi, A. S. Mansoor, U. K. Radi and R. Wahab, *Plasmonics*, 2024, DOI: **10.1007/s11468-024-02481-4**.
8 S. Abdullaev, D. Singh, M. N. Al-Delfi, A. Kumar, Q. H. Aziz, A. Elawady, M. A. Al-Anber, A. H. Al-Rubaye, A. Ali and N. Ahmad, *Appl. Organomet. Chem.*, 2024, **38**, 7245.
9 A. Ali, J. M. Moradian, A. Naveed, S. N. Uz-Zaman Haider, J. Lu, S. S. A. Shah, H. Ahmed Keerio, W. Ahmad Qureshi, H. Naz, R. Wahab, F. Zhiqiang and L. Guo, *J. Catal.*, 2024, **438**, 115729.
10 V. V. Costa, M. Estrada, Y. Demidova, I. Prosvirin, V. Kriventsov, R. F. Cotta, S. Fuentes, A. Simakov and E. V. Gusevskaya, *J. Catal.*, 2012, **292**, 148–156.
11 C. J. Jia, Y. Liu, H. Bongard and F. Schüth, *J. Am. Chem. Soc.*, 2010, **132**, 1520–1522.
12 B. R. Cuenya, *Thin Solid Films*, 2010, **518**, 3127–3150.
13 S. Li, H. Zhu, Z. Qin, G. Wang, Y. Zhang, Z. Wu, Z. Li, G. Chen, W. Dong, Z. Wu, L. Zheng, J. Zhang, T. Hu and J. Wang, *Appl. Catal., B*, 2014, **144**, 498–506.
14 W. Yan, B. Chen, S. M. Mahurin, V. Schwartz, D. R. Mullins, A. R. Lupini, S. J. Pennycook, S. Dai and S. H. Overbury, *J. Phys. Chem. B*, 2005, **109**, 10676–10685.
15 W. Yan, B. Chen, S. M. Mahurin, S. Dai and S. H. Overbury, *Chem. Commun.*, 2004, **77**, 1918–1919.
16 K. Y. Ho and K. L. Yeung, *Gold Bull.*, 2007, **40**, 15–30.
17 M. P. Casaletto, A. Longo, A. Martorana, A. Prestianni and A. M. Venezia, *Surf. Interface Anal.*, 2006, **38**, 215–218.
18 A. N. Pestryakov and V. V. Lunin, *Mol. Catal.*, 2000, **158**, 325–329.
19 A. Abad, P. Concepción, A. Corma and H. García, *Angew. Chem.*, 2005, **117**, 4134–4137.
20 X. Y. Wang, S. P. Wang, S. R. Wang, Y. Q. Zhao, J. Huang, S. M. Zhang, W. P. Huang and S. H. Wu, *Catal. Lett.*, 2006, **112**, 115–119.
21 S. Carrettin, P. Concepción, A. Corma, J. M. López Nieto and V. F. Puntes, *Angew. Chem., Int. Ed.*, 2004, **43**, 2538–2540.
22 M. Hisamoto, R. C. Nelson, M.-Y. Lee, J. Eckert and S. L. Scott, *J. Phys. Chem. C*, 2009, **113**, 8794–8805.
23 K. Bourikas, C. Kordulis and A. Lycourghiotis, *Catal. Rev.*, 2006, **48**, 363–444.
24 J. Huang, Y. Wang, J. Zheng, W.-L. Dai and K. Fan, *Appl. Catal., B*, 2011, **103**, 343–350.
25 K. Wefers, *Alcoa Technical Paper*, 1987, p. 19.
26 J. Wang, A. H. Lu, M. Li, W. Zhang, Y. S. Chen, D. X. Tian and W. C. Li, *ACS Nano*, 2013, **7**, 4902–4910.
27 V. F. Anufrienko, B. L. Moroz, T. V. Larina, S. P. Ruzankin, V. I. Bukhtiyarov and V. N. Parmon, *Dokl. Phys. Chem.*, 2007, **413**, 75–80.
28 S. B. Erenburg, B. L. Moroz, N. V. Bausk, V. I. Bukhtiyarov and S. Nikitenko, *Nucl. Instrum. Methods Phys. Res., Sect. A*, 2007, **575**, 105–108.
29 B. L. Moroz, P. A. Pyrjaev, V. I. Zaikovskii and V. I. Bukhtiyarov, *Catal. Today*, 2009, **114**, 292–305.
30 Z. Shi, W. Jiao, L. Chen, P. Wu, Y. Wang and M. He, *Microporous Mesoporous Mater.*, 2016, **224**, 253–261.
31 W. Q. Jiao, X. M. Liang, Y. M. Wang and M. Y. He, *CrystEngComm*, 2014, **16**, 3348–3358.
32 J. Zhang, S. Liu, J. Lin, H. Song, J. Luo, E. M. Elssfah, E. Ammar, Y. Huang, X. Ding, J. Gao, S. Qi and C. Tang, *J. Phys. Chem. B*, 2006, **110**, 14249–14252.
33 S. Lowell, J. E. Shields, M. A. Thomas and M. Thommes, *Characterization of Porous Solids and Powders: Surface Area, Pore Size and Density*, Kluwer Academic Publishers, Dordrecht, 2004.
34 J. Zhang, S. Wei, J. Lin, J. Luo, S. Liu, H. Song, E. Elawad, X. Ding, J. Gao, S. Qi and C. Tang, *J. Phys. Chem. B*, 2006, **110**, 21680–21683.
35 J. H. Kwak, J. Hu, D. Mei, C.-W. Yi, D. H. Kim, C. H. F. Peden, L. F. Allard and J. Szanyi, *Science*, 2009, **325**, 1670–1673.
36 J. García-Serrano, A. G. Galindo and U. Pal, *Sol. Energy Mater. Sol. Cells*, 2004, **82**, 291–298.
37 M. S. Ide and R. J. Davis, *Acc. Chem. Res.*, 2014, **47**, 825–833.
38 W. Tang, J. Weng, X. Lu, L. Wen, A. Suburamanian, C. Y. Nam and P. X. Gao, *Appl. Catal., B*, 2019, **256**, 117859.
39 A. C. Gluhoi and B. E. Nieuwenhuys, *Catal. Today*, 2007, **122**, 226–232.
40 G. Li, Y. Liu, D. Liu, L. Liu and C. Liu, *Mater. Res. Bull.*, 2010, **45**, 1487–1491.
41 R. M. Silverstein, G. C. Bassler and T. C. Morrill, *J. Chem. Educ.*, 2014, **92**, 826–827.
42 K. Shin-Ya, H. Sugeta, S. Shin, Y. Hamada, Y. Katsumoto and K. Ohno, *J. Phys. Chem. A*, 2007, **111**, 8598–8605.
43 D. L. Pavia, G. M. Lampman, G. S. Kriz and J. A. Vyvyan, *Introduction to Spectroscopy*, 4th edn, 2009.
44 M. C. Kung, R. J. Davis and H. H. Kung, *J. Phys. Chem. C*, 2007, **111**, 11767–11775.
45 J. Chen, Q. Zhang, Y. Wang and H. Wan, *Adv. Synth. Catal.*, 2008, **350**, 453–464.
46 K. Yamaguchi and N. Mizuno, *Angew. Chem., Int. Ed.*, 2002, **41**, 4538–4542.
47 D. E. Jiang, S. H. Overbury and S. Dai, *J. Phys. Chem. Lett.*, 2011, **2**, 1211–1215.